

Exceptional Points in Gyrator-Based Circuit and Nonlinear High-Sensitivity Oscillator

Alireza Nikzamir, Kasra Rouhi, Alexander Figotin, and Filippo Capolino

Abstract—We present a scheme for high-sensitive oscillators based on an exceptional point of degeneracy (EPD) in a circuit made of two LC resonators coupled by a gyrator. The frequency of oscillation is very sensitive to perturbations of a circuit element, like a capacitor. We show conditions that lead to an EPD, assuming one of the two resonators is composed of an inductor and a capacitor of negative values. The EPD occurrence and sensitivity to perturbations in the linear case are demonstrated by showing that the eigenfrequency bifurcation around the EPD is described by the relevant Puiseux (fractional power) series expansion. We also investigate the effect of small losses in the system and show that they lead to instability. We fabricate the circuit, and exploit its instability and nonlinearity, observing experimentally stable self-oscillations under the saturated regime. We measure the circuit’s sensitivity to a small capacitor perturbation. A shift in frequency of oscillation after saturation is well detectable with very distinct spectral peaks with 10 Hz linewidth, clean until -70 dB from the peak value. The sensitivity is (i) higher than the one of a comparable simple LC linear resonator, (ii) comparable or better than other published EPD circuits, and (iii) applicable to both negative and positive values of the capacitance perturbation, contrary to what happens in PT-symmetric circuits. The proposed scheme can pave the way for a new generation of high-sensitive sensors to measure slight variations in physical, chemical or biological quantities.

Index Terms—Coupled resonators, exceptional point of degeneracy (EPD), gyrator, nonlinear, perturbation theory, sensor

I. INTRODUCTION

RECENT advancements associated with the concept of exceptional points of degeneracy (EPDs) have attracted a surge of interest due to their potential for various applications. An EPD is a point in the parameter space of a system for which the eigenvalues and the eigenvectors of the relevant matrix coalesce [1], [2], [3], [4], [5], [6], [7], [8], [9]. The EPD concept has been investigated in temporally periodic electric and mechanical systems [10], [11], in coupled-resonator systems with loss and/or gain under parity-time symmetry [12], [7], [13], [14]. The EPD concept using saturable nonlinear gain has been exploited in conceiving oscillators based on two coupled transmission line [14], [15] and two resonator circuits [16]. Since the characterizing feature of an exceptional point is the full degeneracy of at least two eigenmodes, as mentioned in [17], the significance of referring to it as “degeneracy” is here emphasized, hence including the D in EPD. In essence, an EPD is obtained when the system matrix associated to a

linear system is similar to a matrix that comprises a non-trivial Jordan block. In recent years, frequency splitting phenomena at EPDs have been proposed for sensing applications [18], [19], [20]. Frequency splitting occurs at degenerate resonance frequencies where system eigenmodes coalesce. Such a degenerate resonance frequency is extremely sensitive to a small perturbation in system parameters. This perturbation leads to a shift in the system resonance frequency that can be detected and measured. This concept has been exploited in new sensing schemes such as optical microcavities [21], optical gyroscopes [22], [23] and mass sensor [24]. Recently, EPD in nonlinear systems has gained interest by showing its potential in advancing sensing technologies and stability analysis. These studies [25], [26] illustrate how nonlinear dynamics at EPDs enhance sensor sensitivity and signal-to-noise ratio and pave the way for innovative electronic system designs, underlining EPDs’ critical role in sensing applications.

It has been recently shown that negative capacitors and inductors are useful to realize EPDs in a system made of two resonators coupled via a gyrator [27], [28], [29], [30]. These non-passive negative reactive components are synthesized with negative impedance converters (NICs) or negative impedance inverters (NIIs), which produce a negative capacitor or a negative inductor with feedback circuits [31]. Negative capacitances and inductances are largely used in electronics where negative capacitors are obtained with op amps [32], [33] or with other semiconductor devices [34]. Negative inductances were obtained as early as 1965 using a grounded NII [32], and various circuits have been proposed for floating negative inductance using different types of op amps for operation below 1 MHz. An ideal gyrator is a two-port network that transforms a current into a voltage and vice versa and causes 180 degrees phase shift difference in the signal transmission from one side to the other [35]. Gyrators have been designed using operational amplifiers (op amps) [36] or microwave circuits [37].

In this paper, we explore for the first time the saturation regime due to the nonlinearity in active negative inductance and negative capacitance, in an EPD resonator topology based on a gyrator, and explore the measured high sensitivity. We describe several EPD features in gyrator-based coupled resonant circuits, where two LC resonators (series-series and parallel-parallel configurations) are coupled to each other through a gyrator. We illustrate the necessary conditions to obtain the EPD in both parallel and series resonant circuit configurations and show the signal behavior using time domain simulations. We also provide a frequency domain analysis in terms of phasors and show that the EPD corresponds to a double zero

Alireza Nikzamir, Kasra Rouhi, and Filippo Capolino are with the Department of Electrical Engineering and Computer Science, University of California, Irvine, CA 92697 USA, e-mails: anikzami@uci.edu, kasra.rouhi@uci.edu, and f.capolino@uci.edu.

Alexander Figotin is with the Department of Mathematics, University of California, Irvine, CA 92697 USA, e-mail: afigotin@uci.edu.

of the total impedance defining the resonance. Importantly, we discuss the effect of additional losses in the system and show how they make the circuit unstable. The effect of the circuit's nonlinearities is observed experimentally after saturation is achieved, leading to a stable oscillatory regime. When the system is perturbed away from its EPD, the self-oscillation frequency is shifted, and such a shift is measured to determine the circuit's sensitivity. Compared to our previous studies in [27], [28], [29], [30], we focus on the analysis of the series-series configuration including losses that we did not explore before; we also analyze a parallel-parallel configuration, and fabricate a gyration-based circuit for the first time. We then observe experimentally the self oscillatory regime under saturation and perturb a capacitance value to measure the oscillation frequency shifts. In addition, we compare the sensitivity of our proposed circuit to previous linear and nonlinear circuits supporting EPD [13], [16], [10], [15], highlighting how its sensitivity is comparable and emphasizing the capability of detecting small perturbations. The proposed circuit and method have promising applications in ultrasensitive sensors at various operating frequencies.

II. EPD IN PARALLEL CONFIGURATION

We show a configuration in which we get an EPD by using a gyration-based circuit. Two parallel resonators are utilized in two different lossy/lossless configurations. We briefly introduce the gyration element and later on, we write the required circuit equations in the Liouvillian formalism. Then, we solve the eigenvalue problem to calculate the resonant frequencies (i.e., the eigenfrequencies) and determine the conditions for obtaining EPD at a desired frequency in a lossy circuit. We discuss the conditions for real-valued EPD frequency and stability in the system. In order to provide a comprehensive analysis of the presented circuit and its stability, in Section II-B, we study the eigenfrequencies in the lossless resonators, and we verify our theoretical calculations by using a time-domain circuit simulator (Keysight Advanced Design System (ADS)). Then, we provide an example and the eigenfrequency dispersion with respect to changes in parameters and we show the perturbation effects on the circuit's eigenfrequencies.

A. EPD in Lossy Parallel Circuit

The gyration is a passive, linear, lossless, nonreciprocal, two-port electrical element. It allows network realizations of devices that cannot be realized with the conventional four components (i.e., resistors, inductors, capacitors, and transformers) [35], [38]. An important property of a gyration is that it inverts the current-voltage characteristic; therefore, an impedance load is also inverted across the gyration. In other words, a gyration can make a capacitive circuit behave inductively, and a series LC circuit behaves like a parallel LC circuit. The instantaneous voltages and currents on the gyration ports are related by [35]

$$\begin{cases} v_2 = R_g i_1 \\ v_1 = -R_g i_2 \end{cases} \quad (1)$$

where the gyration resistance R_g is the important parameter in the ideal gyration. In the parallel-parallel configuration, two

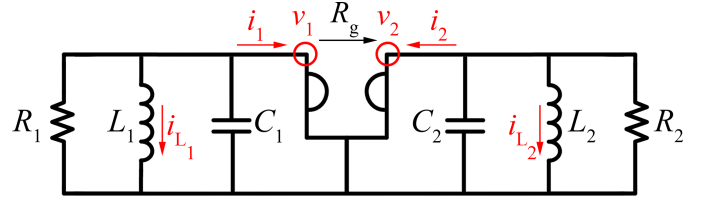


Fig. 1. Schematic view of the lossy parallel-parallel configuration including losses in each resonator. Inductance and capacitance are negative in the right resonator.

parallel RLC resonators are coupled by a gyration as displayed in Fig. 1. We find the EPD condition in this circuit by writing the Kirchhoff current law equations and finding the associated Liouvillian matrix. Hence, we assume that all components are ideal, and inductors and capacitors contain no additional resistance. We write the two Kirchhoff current law equations and by using the state vector as, $\Psi \equiv [Q_1, Q_2, \dot{Q}_1, \dot{Q}_2]^T$, where Q_n is the stored charge in the capacitor C_n ($n = 1$ for the left resonator and $n = 2$ for the right resonator), and the superscript T denotes the transpose operation. The circuit dynamics are described based on the Liouvillian formalism as

$$\frac{d\Psi}{dt} = \underline{\mathbf{M}}\Psi, \quad \underline{\mathbf{M}} = \begin{pmatrix} 0 & 0 & 1 & 0 \\ 0 & 0 & 0 & 1 \\ -\omega_{01}^2 & 0 & -\gamma_1 & \frac{1}{R_g C_2} \\ 0 & -\omega_{02}^2 & -\frac{1}{R_g C_1} & -\gamma_2 \end{pmatrix}, \quad (2)$$

where $\underline{\mathbf{M}}$ is the 4×4 circuit matrix, and $\gamma_1 = 1/(R_1 C_1)$ and $\gamma_2 = 1/(R_2 C_2)$ represent the resonators loss parameter (losses on the right resonator are represented by a negative γ_2 since C_2 is negative). Furthermore, $\omega_{01} = 1/\sqrt{C_1 L_1}$, and $\omega_{02} = 1/\sqrt{C_2 L_2}$ are resonance angular frequencies of two isolated left and right resonators, assumed to be both real (the case where they are imaginary is shown in Ref. [29]). Assuming signals of the form $Q_n \propto e^{j\omega t}$, we write the associated eigenvalue problem, and the characteristic equation is obtained from $\det(\underline{\mathbf{M}} - j\omega \underline{\mathbf{I}}) = 0$, where $\underline{\mathbf{I}}$ is the identity matrix, leading to

$$\begin{aligned} \omega^4 - j\omega^3(\gamma_1 - \gamma_2) - \omega^2 \left(\omega_{01}^2 + \omega_{02}^2 + \gamma_1 \gamma_2 + \frac{1}{R_g C_1 C_2} \right) \\ + j\omega(\gamma_1 \omega_{02}^2 + \gamma_2 \omega_{01}^2) + \omega_{01}^2 \omega_{02}^2 = 0. \end{aligned} \quad (3)$$

The coefficients of the odd-power terms of the angular eigenfrequency (ω and ω^3) in the characteristic equation of Eq. (3) are imaginary. Eigenfrequencies ω and $-\omega^*$ are both roots. In order to have a stable circuit with real-valued eigenfrequencies, the odd-power terms of the angular eigenfrequency $-j\omega^3(\gamma_1 - \gamma_2)$ and $j\omega(\gamma_1 \omega_{02}^2 + \gamma_2 \omega_{01}^2)$ in the characteristic equation of Eq. (3) should be zero. The coefficient of the ω^3 term is zero when $\gamma_1 = \gamma_2$. We recall that γ_2 is negative, so the condition $\gamma_1 = \gamma_2$ happens either in absence of losses or when one resonator has gain. However, under this latter gain condition enabling $\gamma_1 = \gamma_2$, the coefficient of the ω term $\gamma_1(\omega_{02}^2 + \omega_{01}^2)$ is non-zero because ω_{01}^2 and ω_{02}^2 are both positive, and also in this case it would not be possible to have

purely real eigenfrequencies. On the other hand, the coefficient of the ω term vanishes when $\gamma_1/\gamma_2 = -\omega_{01}^2/\omega_{02}^2$, and under this condition, the coefficient of the ω^3 term $\gamma_1(1 + \omega_{02}^2/\omega_{01}^2)$ cannot vanish. In summary, it is not possible to have all real-valued coefficients in the characteristic polynomials, unless $\gamma_1 = \gamma_2 = 0$, which corresponds to a lossless circuit. In other words, under any amount of small loss, there is no condition to make both ω and ω^3 coefficients equal to zero, hence the eigenfrequencies are complex, leading to instabilities that cause oscillations. In the following subsection, we analyze the eigenfrequency in a lossless structure to further understand the stability of the lossless structure.

B. EPD in Lossless Parallel Circuit

To meet the EPD condition for real valued eigenfrequency, we assume $\gamma_1 = \gamma_2 = 0$. Accordingly, the circuit consists of two lossless parallel LC resonators coupled by a gyration. The eigenfrequencies for this case are found by solving

$$\omega^4 - \omega^2 \left(\omega_{01}^2 + \omega_{02}^2 + \frac{1}{C_1 C_2 R_g} \right) + \omega_{01}^2 \omega_{02}^2 = 0. \quad (4)$$

All the ω 's coefficients are real hence ω and ω^* are both roots of the characteristic equation. Moreover, it is a quadratic equation in ω^2 , therefore ω and $-\omega$ are both solutions. The system's angular eigenfrequencies are

$$\omega_{1,3} = \pm\sqrt{a+b}, \quad \omega_{2,4} = \pm\sqrt{a-b}, \quad (5)$$

$$a = \frac{1}{2} \left(\omega_{01}^2 + \omega_{02}^2 + \frac{1}{C_1 C_2 R_g} \right), \quad (6)$$

$$b^2 = a^2 - \omega_{01}^2 \omega_{02}^2. \quad (7)$$

The EPD is obtained when the resonance frequencies of the circuit coalesce, i.e., when

$$b = 0, \quad (8)$$

which happens when $a^2 = \omega_{01}^2 \omega_{02}^2$. The positive EPD angular frequency is then given by $\omega_e = \sqrt{a}$, where we assume $a > 0$. The condition to obtain real value for EPD frequency is rewritten as

$$\omega_{01}^2 + \omega_{02}^2 - \omega_{gp}^2 > 0, \quad (9)$$

where it has been convenient to define $\omega_{gp}^2 = -1/(C_1 C_2 R_g)$ for the parallel-parallel configuration (note that $\omega_{gp}^2 > 0$ because one capacitor is negative). When both Eq. (8) and inequality in (9) are satisfied, two eigenfrequencies coalesce at a real EPD angular frequency,

$$\omega_e = \sqrt{\frac{1}{2} (\omega_{01}^2 + \omega_{02}^2 - \omega_{gp}^2)} = \sqrt{\omega_{01} \omega_{02}}. \quad (10)$$

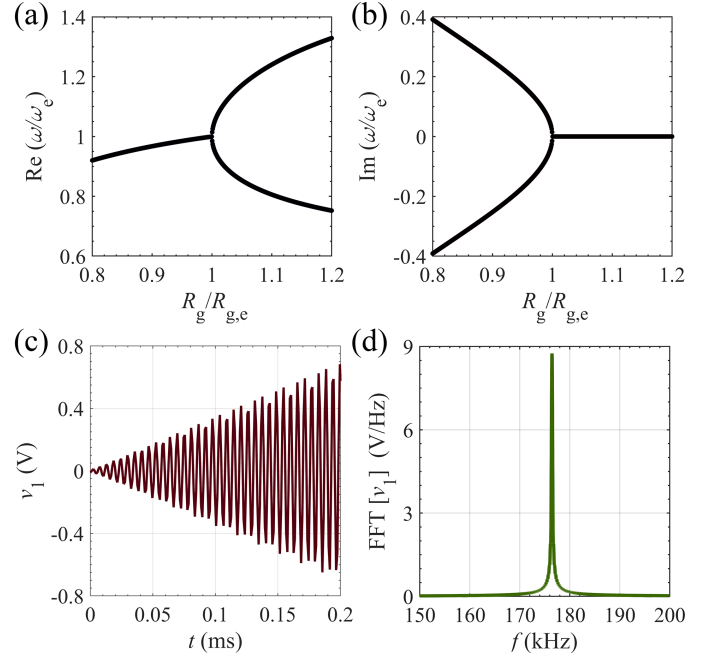


Fig. 2. Variation of the (a) real and (b) imaginary parts of the two eigenfrequencies to a gyration resistance perturbation in the lossless parallel-parallel configuration. The bifurcation in the real part is observed for $R_g > R_{g,e}$. Voltage v_1 under the EPD condition in the (c) time domain, and (d) frequency domain. The frequency domain result is calculated from 150 kHz to 200 kHz performing an FFT with 10^6 samples in the time window between 0 ms to 0.2 ms.

C. Dispersion Relation of Lossless and Lossy Parallel-parallel Configurations

As an example, we use the following values: $L_1 = 47 \mu\text{H}$, $L_2 = -47 \mu\text{H}$, $C_2 = -47 \text{nF}$, and $R_g = 50 \Omega$. We then obtain two values of capacitance $C_{1,e} = 6.34 \text{nF}$ and $C_{1,e} = 125.25 \text{nF}$ by imposing Eq. (8) to be satisfied. Here, both capacitors lead to $a > 0$, enabling the EPD angular frequency to be real valued. Indeed, the $C_{1,e} = 6.34 \text{nF}$ leads to $\omega_e = 1.11 \times 10^6 \text{ rad/s}$, whereas $C_{1,e} = 125.25 \text{nF}$ leads to $\omega_e = 5.26 \times 10^5 \text{ rad/s}$. In the following we use $C_{1,e} = 6.34 \text{nF}$. The results in Figs. 2(a) and (b) show the branches of the real and imaginary parts of perturbed eigenfrequencies obtained from the eigenvalue problem when varying the gyration resistance near $R_{g,e} = 50 \Omega$. The bifurcation of the real part in this case happens for $R_g > R_{g,e}$. Perturbing other components like C_1 or L_1 leads to analogous results.

The time domain simulation result for the node voltage v_1 in Fig. 2(c) is obtained using the Keysight ADS circuit simulator by employing the ideal model for the gyration, using the above circuit values that lead to the EPD. We assume the capacitor has an initial voltage on C_1 equal to 1 mV. The voltage grows linearly with increasing time, demonstrating two eigenvalues of the circuit are coalescing, and the system exhibits a double pole, as shown later on. This is peculiar of a second-order EPD. The spectrum of the voltage v_1 in Fig. 2(d) is calculated after performing the FFT. The oscillation frequency is $f_o = 176.66 \text{ kHz}$, which is the EPD frequency calculated above.

By perturbing the gyration resistance, the circuit no longer operates at EPD. For a higher gyration resistance value, $R_g =$

$52.5 \Omega > R_{g,e} = 50 \Omega$ as a 5% increase, we obtain two distinct real-valued eigenfrequencies in the system. Thus, we could estimate the amount of perturbation in R_g by measuring the frequency of these two resonances. On the other hand, by reducing the amount of perturbed parameter by 5%, leading to $R_g = 47.5 \Omega < R_{g,e} = 50 \Omega$, the system has two complex eigenfrequencies with non-zero imaginary parts. The circuit contains signals that are damping or growing exponentially.

In the lossy circuit, we use the same values of lossless parallel-parallel configuration for the resonators and gyration resistance plus the two resistances. In Figs. 3(a) and (b), we vary γ_1 and assume $\gamma_2 = 0$, whereas in Figs. 3(c) and (d), we perturb $-\gamma_2$ and assume $\gamma_1 = 0$. In fact, when we vary γ_1 or γ_2 , we actually vary R_1 or R_2 , while keeping constant C_1 and C_2 . When $\gamma_1 = \gamma_2 = 0$, the EPD frequency is the same as the one found earlier for the lossless configuration in Section II-B. Figures 3(a)-(d) show the bifurcation of the real and imaginary parts of eigenfrequencies on both sides of the EPD. It means that the circuit is very sensitive to both positive and negative variations in the resistance value. The angular eigenfrequencies are complex-valued for any amount of loss and the circuit is in the self-oscillation regime. The circuit's signal oscillates with the frequency associated with the real part of the unstable eigenfrequency, and the signal grows exponentially based on the unstable imaginary part of the eigenfrequency. The calculated results show that we achieve higher sensitivity when perturbing γ_2 .

D. Parallel Lossless Circuit Sensitivity

The degenerate eigenvalue (resonance frequency) at an EPD is exceedingly sensitive to perturbations of system parameters. Here, we show that the sensitivity of a system's observable to a specific variation of a component's value is large because of EPD. Let us consider the parallel-parallel configuration in the EPD regime, with the values of the components given in Section II-B. We select the parallel case because all elements are grounded and this sometimes represents a simplification when using realistic active components that require biasing (for more information on dispersion relation for series-series configuration you can refer to the Appendix V-A). For simplicity, we discuss the case without resistances and we define the relative circuit perturbation Δ_X as

$$\Delta_X = \frac{X - X_e}{X_e}, \quad (11)$$

where X is the perturbed value of a component and X_e is the unperturbed value that provides the EPD. The subscript "X" denotes the perturbed parameter. In this section, we consider variations of C_1 and L_1 , one at a time, in the lossless configuration. The calculated diagrams for the real and imaginary parts of the eigenfrequencies near the EPD are shown in Fig. 4. We conclude that the individual variation of the parameters of C_1 or L_1 show similar sensitivity behavior, i.e., the real part of the eigenfrequencies splits for $\Delta_X < 0$. Note that the L_1 perturbation shows higher sensitivity because of the wider bifurcation in the dispersion diagram.

We explain the extreme sensitivity by resorting to the general theory of EPDs. Note that after applying a perturbation

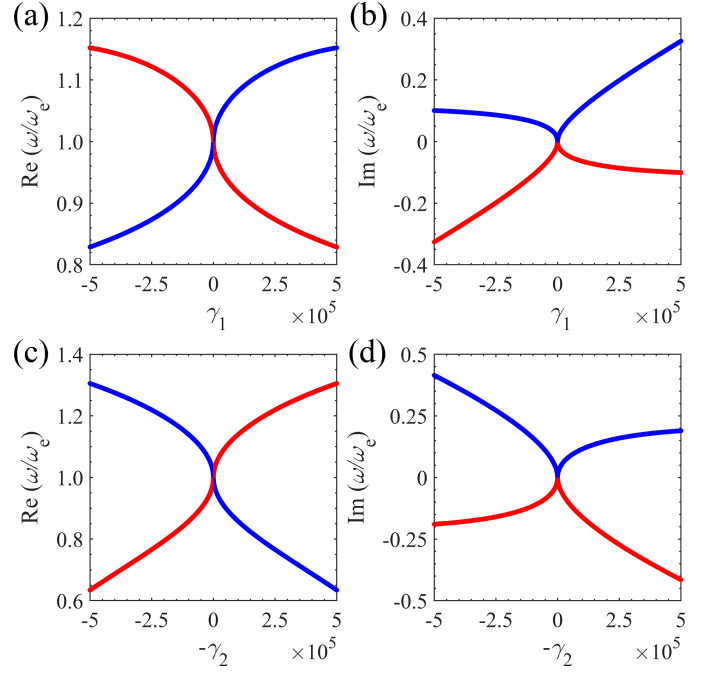


Fig. 3. Variation of (a) real and (b) imaginary parts of the angular eigenfrequencies to a resistor perturbation on the left resonator. In these plots, γ_1 is varied whereas we assume $\gamma_2 = 0$. Variation of (c) real and (d) imaginary parts of the angular eigenfrequencies to a resistor perturbation on the right resonator. In these plots, $-\gamma_2$ is varied whereas we assume $\gamma_1 = 0$. In these plots, blue curves show stable branches with positive imaginary parts and red curves show unstable branches with negative imaginary parts. In addition, the right half of each plot demonstrates the variation in eigenfrequencies due to varying positive resistance, whereas the left half demonstrates the variation in eigenfrequencies due to varying negative resistance.

in Δ_X value, we will have a perturbed matrix $\underline{\mathbf{M}}(\Delta_X)$. Consequently, the two degenerate eigenvalues at the EPD change considerably due to the small perturbation in Δ_X , resulting in two distinct eigenfrequencies $\omega_p(\Delta_X)$, with $p = 1, 2$. A single convergent Puiseux series is used to represent the two perturbed eigenvalues near an EPD, where the coefficients are calculated using the explicit recursive formulas presented in [39]. An approximation of $\omega_p(\Delta_X)$ around a second-order EPD is given by

$$\omega_p(\Delta_X) \approx \omega_e + (-1)^p \alpha_1 \sqrt{\Delta_X} + \alpha_2 \Delta_X. \quad (12)$$

Following [39], we calculate the coefficients as

$$\alpha_1 = \sqrt{-\frac{\frac{\partial H(\Delta_X, \omega)}{\partial \Delta_X}}{\frac{1}{2!} \frac{\partial^2 H(\Delta_X, \omega)}{\partial \omega^2}}}, \quad (13)$$

$$\alpha_2 = -\frac{\alpha_1^3 \frac{1}{3!} \frac{\partial^3 H(\Delta_X, \omega)}{\partial \omega^3} + \alpha_1 \frac{\partial^2 H(\Delta_X, \omega)}{\partial \omega \partial \Delta_X}}{\alpha_1 \frac{\partial^2 H(\Delta_X, \omega)}{\partial \omega^2}}, \quad (14)$$

evaluated at the EPD, i.e., at $\Delta_X = 0$ and $\omega = \omega_e$, where $H(\Delta_X, \omega) = \det[\underline{\mathbf{M}}(\Delta_X) - j\omega \underline{\mathbf{I}}]$. Equation (12) indicates that for a small perturbation $\Delta_X \ll 1$, the eigenvalues change dramatically from their original degenerate value due to the square root function. In the first example, the perturbed parameter is the positive capacitance on the left resonator, $\Delta_C = (C_1 - C_{1,e})/C_{1,e}$, and the Puiseux series first-order

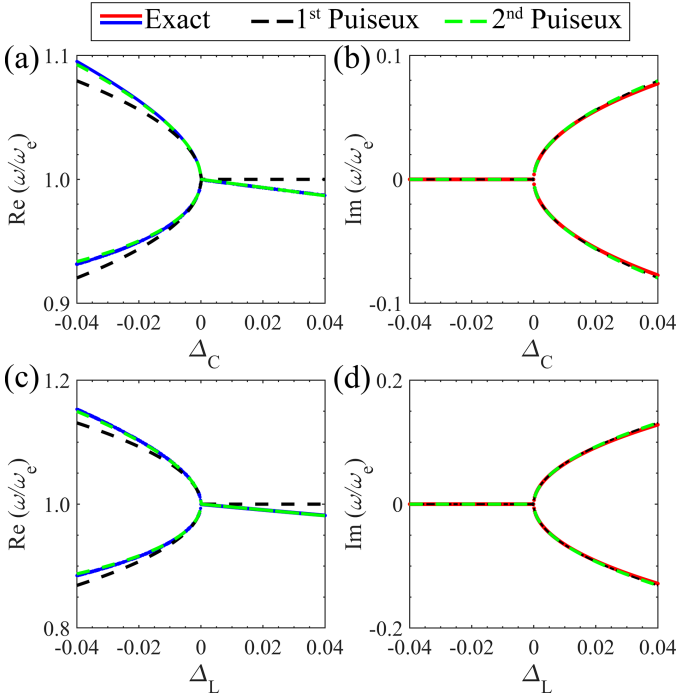


Fig. 4. High sensitivity of the (a) real and (b) imaginary parts of the eigenfrequencies to relative capacitance perturbation $\Delta_C = (C_1 - C_{1,e})/C_{1,e}$. The two perturbed frequencies are real for $\Delta_C < 0$. High sensitivity of the (c) real and (d) imaginary parts of the eigenfrequencies to relative inductance perturbation $\Delta_L = (L_1 - L_{1,e})/L_{1,e}$. The two perturbed frequencies are real for $\Delta_L < 0$.

coefficient is calculated by Eq. (30) as $\alpha_1 = j4.4138 \times 10^5$ rad/s and the second-order coefficient is calculated as $\alpha_2 = -3.6503 \times 10^5$ rad/s. The result in Figs. 4(a) and (b) shows the two branches of the perturbed eigenfrequencies ω obtained directly from the eigenvalue problem (or characteristic equation) when the perturbation Δ_C is applied. This example uses C_1 as a sensing component to detect variation in physical or chemical parameters converted into electrical parameters. However, variation in other components' values can also be used in various realistic scenarios. Figures 4(a) and (b) demonstrate that the perturbed eigenvalues can be estimated with great accuracy by using the Puiseux series truncated at its second order (green dashed lines). We have also shown the first-order approximation in Figs. 4(a) and (b) for better comparison (black dashed lines), which is also in good agreement with the eigenfrequencies obtained by the characteristic equation. For a small positive value of Δ_C , the imaginary parts of the eigenfrequencies experience a sharp change, while their real parts remain more or less constant. A small negative value of Δ_C causes a rapid variation in the real part of the eigenfrequencies.

In the second example, the perturbed parameter is the positive inductance on the left resonator, $\Delta_L = (L_1 - L_{1,e})/L_{1,e}$, and the Puiseux series first-order coefficient is calculated by Eq. (31) as $\alpha_1 = j7.2792 \times 10^5$ rad/s and the second-order coefficient is calculated as $\alpha_2 = -5.1598 \times 10^5$ rad/s. The calculated results in Fig. 4(c) and (d) show the two branches of the perturbed eigenfrequencies obtained from the eigenvalue problem when the perturbation in inductance is applied. By

applying the Puiseux series truncated at its second order, it is possible to estimate the perturbed eigenfrequencies with high accuracy. However, the first order also provides relatively accurate results. The imaginary parts of the eigenfrequencies undergo a sharp change for very small positive perturbations, while their real parts remain relatively unchanged. A small negative perturbation in the inductor value causes rapid variation in the eigenfrequencies' real part. This feature is one of the most extraordinary physical properties associated with the EPD and it can be exploited for designing ultra-sensitive sensors [40].

E. Frequency Domain Analysis of The Degenerate Resonance

We show how the EPD regime is associated to a special kind of circuit's resonance, directly observed in a frequency domain analysis of the circuit. We calculate the total input admittance, $Y_{\text{total}}(\omega)$ (see Fig. 5(a)), for the parallel-parallel circuit by finding the transferred impedance $Y_{\text{trans}}(\omega)$ on the left side of the circuit. We define the two admittances of the resonators as $Y_1 = j\omega C_1 + 1/(j\omega L_1)$, $Y_2 = j\omega C_2 + 1/(j\omega L_2)$, and calculate the transferred admittance on the left side as

$$Y_{\text{trans}}(\omega) = \frac{1}{R_g^2 Y_2}. \quad (15)$$

The total admittance $Y_{\text{total}}(\omega)$ is calculated as

$$Y_{\text{total}}(\omega) \triangleq Y_1(\omega) + Y_{\text{trans}}(\omega) = Y_1 + \frac{1}{R_g^2 Y_2}. \quad (16)$$

The resonant angular frequencies are obtained imposing $Y_{\text{total}}(\omega) = 0$. A few steps lead to the same ω -zeros given by Eq. (5). We calculate the resonance frequencies for various gyration resistance values in Fig. 5(b). When considering the EPD gyration resistance $R_g = R_{g,e} = 50 \Omega$, one has $Y_{\text{total}}(\omega) \propto (\omega - \omega_e)^2$, i.e., the two zeros coincide, represented by the point where the two curves meet exactly at EPD angular frequency. For $R_g < R_{g,e}$, resonance angular frequencies are complex conjugate pairs and for $R_g > R_{g,e}$, the resonance angular frequencies are purely real, consistent with the results in Fig. 2(a) and (b).

III. EXPERIMENTAL SENSITIVITY IN THE SATURATED REGIME

We explore experimentally what happens in the proposed second-order EPD circuit due to unavoidable instabilities, and we actually exploit them by making an oscillator. The key experimental observations are that we have stable oscillations after reaching saturation and the oscillation frequency exhibits high sensitivity to perturbations. We also show that such sensitivity is higher than that of a perturbed single LC resonator. We begin with the linear case, detailing the design of the different components in the circuit. Furthermore, we test the proposed circuit for each part, such as the gyration implementation with op amps. Next, we study the gyration-based circuit in the saturation regime, where the oscillation occurs due to the nonlinearity induced by op amps and losses/gains in each resonator. Finally, we analyze the circuit's sensitivity to

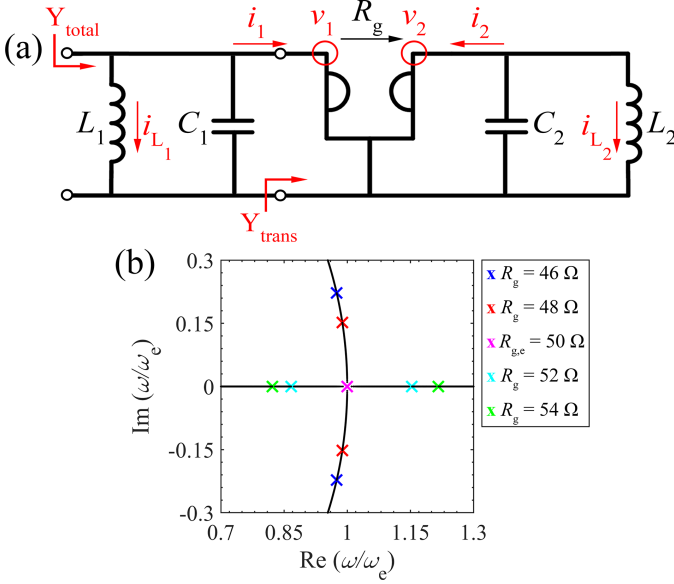


Fig. 5. (a) Schematic view of the lossless parallel-parallel configuration. (b) Root locus of zeros of Y_{total} shows the real and imaginary parts of resonance frequencies of the parallel configuration when varying gyration resistance. The EPD frequency corresponds to a double zero of the admittance Y_{total} .

capacitance changes. The values for the experiment are set as $C_1 = 400 \text{ nF}$, $L_1 = 47 \mu\text{H}$, $L_2 = -10 \mu\text{H}$ and $C_2 = -470 \text{ nF}$ where these values ideally lead to an EPD at $f = 51.9 \text{ kHz}$.

A. Observation of Instability in The Circuit

The gyration resistance has an associated direction indicated by an arrow in the schematic illustrated in Fig. 6(a). Consider the gyration circuit shown in Fig. 6(b) implemented using two op amps of the same model (Texas Instruments, model TLE2071ACP) and seven resistors. By selecting the proper value for the resistors (i.e., R_g in Fig. 6(b)), we control the gyration parameter R_g . The gyration asymmetric impedance matrix \mathbf{Z}_g is given by Eq. (1). To achieve a gyration $R_g = 10 \Omega$, all the resistances in the circuit shown in Fig. 6(b) are set to the same value of 10Ω . We tested the gyration circuit shown in Fig. 6(b) with different loads to ensure that it works properly. We put a load of $Z_L = 33 \Omega$ on the right port of gyration and measure the transferred impedance on the left port as $Z_{\text{trans}} = 3.56 \Omega$ and $Z_{\text{trans}} = 3.42 \Omega$, at frequency of 10 and 100 kHz, respectively, showing an experimental gyration of approximately 9.3Ω and 9.65Ω , respectively. The impedances are measured with an LCR meter (Keysight, model U1733C).

To satisfy the EPD condition based on the theory discussed in Subsection II-B, the positive capacitance in the experiment C_1 is built by paralleling fixed capacitors with values 220 nF, 150 nF, 22 nF and a trimmer (FTVOGUE, model Variable Capacitance Kit) to reach the value of 400 nF. The inductance L_1 is built by using a commercial inductor of $47 \mu\text{H}$ (Coilcraft, model MSS7348-473) with a series DC loss of 0.15Ω and $\pm 20\%$ tolerances. However, due to tolerances, our chosen inductor had a smaller value than the nominal one. We then tuned the inductance by a series inductor with a value of $1 \mu\text{H}$ (Bourns, model 78F1R0K-TR-RC), reaching the measured value of $46.8 \mu\text{H}$ at 100 kHz.

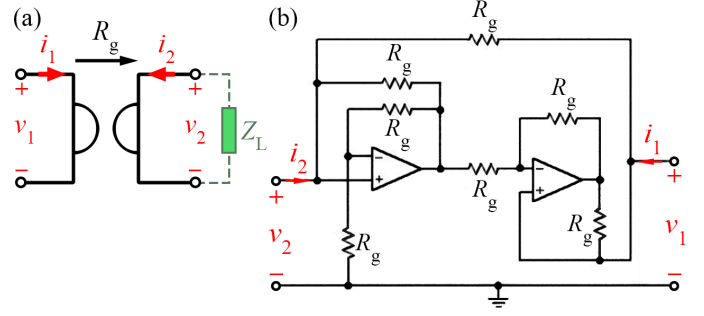


Fig. 6. (a) Gyration schematic and corresponding voltages, currents, and gyration resistance direction. (b) A possible circuit for a gyration implementation by using two op amps and seven resistors.

The negative capacitance and inductance are implemented based on the circuits shown in Appendix V-D using the same op amp model of the gyration. In particular, the negative inductance L_2 is built by using a commercial inductor of $10 \mu\text{H}$ (Coilcraft, model MSS7348-103MEC) with a series DC loss 0.045Ω and $\pm 20\%$ tolerances followed by an inverter in Appendix V-D. However, due to tolerances, our chosen inductor had a smaller value than the nominal one. Then, we tuned the inductance by adding a series inductor with a value of $1 \mu\text{H}$ (Bourns, model 78F1R0K-TR-RC) and a $0.47 \mu\text{H}$ (Bourns, model 542-78FR47K-RC) reaching a measured value of $10.1 \mu\text{H}$ at 100 kHz.

The value of $C_2 = -470 \text{ nF}$ comes from the inverter described in Appendix V-D, where we ignored the gain associated to inversion because of the capacitance's high quality factor. We use a capacitance trimmer (FTVOGUE, model Variable Capacitance Kit) in parallel to a commercial fixed capacitor with a value of 470 nF to achieve a value close to the desired capacitance of 470 nF. All capacitances and inductances are measured with an LCR meter (Keysight, model U1733C) at 100 kHz to ensure the tuning process leads to the desired capacitances and inductances design values. The dispersion diagram of the complex eigenfrequencies by varying the capacitance C_1 is shown in Fig. 7. The system is unstable for any shown value of the perturbed capacitor because of the non-zero imaginary part of eigenfrequencies.

Due to the presence of loss in the prototype, which is caused mainly by the two inductors, we do not have the perfect degeneration of the eigenfrequencies, as shown in Fig. 7(b) where we do not have any more $\text{Im}(f) = 0$ near the bifurcation (plot obtained via simulation in the linear regime). In addition, in the nonlinear regime, the negative inductance and capacitance are responsible of the saturation regime because they act as gain when transferred by the negative impedance converter shown in Appendix V-D. Nevertheless, we can still get in the vicinity of the original EPD frequency.

Since the stored charge in the capacitors is $Q_n \propto e^{j\omega t}$, even a small negative imaginary part of an eigenfrequency leads to an instability and the establishment of self-sustained oscillations, while the charge associated with the other eigenfrequency with positive imaginary part decays. In conclusion, the small gain generated by the inverters leads to non-zero $\text{Im}(f)$, which induces the system state vectors to grow

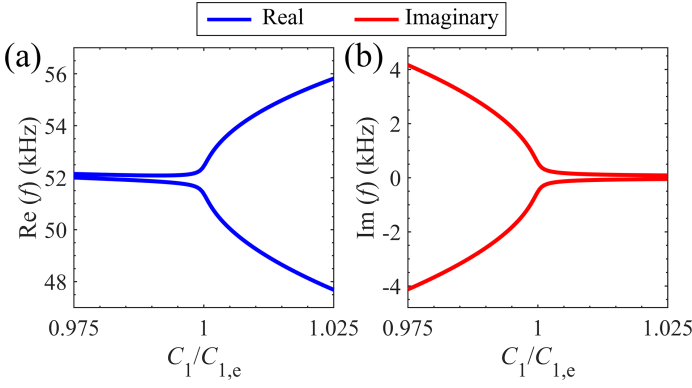


Fig. 7. Variation of (a) real (blue) and (b) imaginary (red) parts of the eigenfrequencies to a capacitance perturbation on the left resonator.

exponentially and it results in an unstable system. We use the instability of the system to our advantage by letting the system oscillate at the EPD frequency, and we investigate the sensitivity of the system in the saturation regime close to the original EPD frequency.

B. Measurements in The Saturation Regime

In the experimental setup, the system saturates exhibiting a steady oscillation at $f_{\text{osc},0} = 50.7\text{kHz}$, measured using a spectrum analyzer (Rigol, model DSA832E), which is close to the frequency shown in Fig. 7 where the bifurcation is imperfect. We observe that the gyration value is close to the designed value of $10\ \Omega$ even after reaching saturation by measuring the voltages v_1 and v_2 in the circuit shown in Fig. 6(a). Also, we considered the transformed admittance of the positive LCR tank after the gyration ($1/Y_{\text{trans}} = R_g^2(C_1 j\omega \parallel 1/(L_1 j\omega + R_1))$) at the frequency of oscillation to find $i_2 = v_2 Y_{\text{trans}}$. As a result, the gyration parameter in the saturated regime at the oscillation frequency of $f_{\text{osc}} = 50.7\text{kHz}$ was calculated as $R_g = 10.8\ \Omega$, which is close to the theoretical design value of $R_g = 10\ \Omega$ and from those measured in the linear regime.

The goal here is to measure the sensitivity of the self oscillation frequency (after reaching saturation) to the perturbation of the capacitance C_1 . Indeed, the measured oscillation frequency dramatically shifts away significantly from the unperturbed frequency $f_{\text{osc},0} = 50.7\text{kHz}$ even when small perturbations are applied. Figure 8(a) shows the experimental time-domain voltage signal v_1 of the capacitor C_1 with respect to the ground, when a relative perturbation $\Delta_C = 2.5\%$ ($\Delta_C = \Delta C/C_{1,0}$, where subscript 0 refers to the unperturbed value of $C_{1,0} = 400\text{ nF}$) is applied to C_1 , measured by an oscilloscope. The voltage frequency is measured with a spectrum analyzer (Rigol DSA832E), and shown in Fig. 8(b), for various C_1 values. A fundamental frequency of oscillation of $f_{\text{osc},0} = 50.7\text{kHz}$ was observed for no perturbation (blue); 49.96kHz for perturbation $\Delta_C = 0.625\%$ (gray); 49.8kHz for perturbation $\Delta_C = 1.25\%$ (green); 49.43kHz for perturbation $\Delta_C = 1.875\%$ (purple); and 48.9kHz for perturbation $\Delta_C = 2.5\%$ (red). We used a resolution bandwidth of 10 Hz , and a video bandwidth of 10 Hz . In all cases, the measured spectrum is clean approximately down -70 dB from the peak values. The linewidths, calculated

at -3 dB from the peak, are approximately 10 Hz which are significantly smaller than the measured frequency shifts. The measured oscillation frequencies versus C_1 are captured in Fig. 8(c) with circles, with the corresponding colors used in Fig. 8(b). In the experiment, a relative perturbation $\Delta_C = 2.5\%$ applied to C_1 in the gyration-based circuit led to a frequency shift $|\Delta f| = |48.9\text{kHz} - 50.7\text{kHz}| = 1.8\text{kHz}$, where $f_{\text{osc},0} = 50.7\text{kHz}$ is the oscillation frequency with no perturbation and $f_{\text{osc}} = 48.9\text{kHz}$ is perturbed oscillation frequency. The measured -3 dB (half power) spectral linewidth of 10 Hz (using a resolution bandwidth of 10 Hz , and a video bandwidth of 10 Hz) is 180 times narrower than the measured frequency shift $|\Delta f| = 1.8\text{kHz}$. For the smallest perturbation of $\Delta_C = 0.625\%$, the associated frequency shift $|\Delta f| = 0.74\text{kHz}$ is 74 times larger than the linewidth of 10 Hz , indicating that the perturbed frequency spectrum is clearly detectable (consider also that the noise floor is 70 dB lower than the peak).

C. Discussion on Sensitivity and Capability to Detect Small Perturbation

We now elaborate on the sensitivity of the gyration-based oscillator in the saturation regime to circuit perturbations and discuss how the obtained experimental results are comparable to those of (i) a single LC resonator in the linear regime, and (ii) other circuits based on EPDs from the literature [13], [10], [16], [15]. In particular, we compare the sensitivity $S = |\Delta_f|/|\Delta_X|$ in the various cases, where $\Delta_f = |\Delta f|/f_0$ and $\Delta_X = |\Delta X|/X_0$ are the normalized changes in the perturbed frequency and a generic parameter X in the circuit (subscript 0 refers to the unperturbed value). The change in the generic parameter X represents changes in capacitance or resistance, as will be discussed next.

We first look at the comparison with a single LC resonator in linear regime, shown in Fig. 8(c), where the variation of the experimental oscillation frequency by perturbing the positive capacitor C_1 (colored circles) of the gyration-based circuit is compared to the resonant frequency shift of a *linear single* LC resonator (dashed black line). The single LC resonator has an inductance $L_s = 24.5\ \mu\text{H}$ and capacitance $C_s = C_1 = 400\text{ nF}$ (same as $C_{1,0}$ value at EPD), with resonance frequency $f_0 = 1/(2\pi\sqrt{L_s C_s}) = 50.8\text{ kHz}$. Perturbing the capacitance C_s leads to a changed frequency of approximately $f \approx f_0(1 - \Delta_{C_s}/2)$, where $\Delta_{C_s} = (C - C_s)/C_s$. The results clearly showcase that the gyration-based circuit in the saturation regime exhibits higher sensitivity compared to that of the linear single LC resonator. Notably, the resonance frequency variation due to the perturbation of capacitance of $\Delta_{C_s} = 10\%$ for the single LC resonator is comparable of the oscillation frequency shift of only $1/8$ of the perturbation ($\Delta_C = 1.25\%$) when using the saturation regime of the gyration-based oscillator. This result shows that the sensitivity of our proposed gyration-based oscillator is 8 times larger than the one of a single LC resonator.

We now compare the sensitivity of the presented oscillator with those obtained using the four circuits in Refs. [13], [10], [16], [15]. In our developed gyration-based circuit, we measured

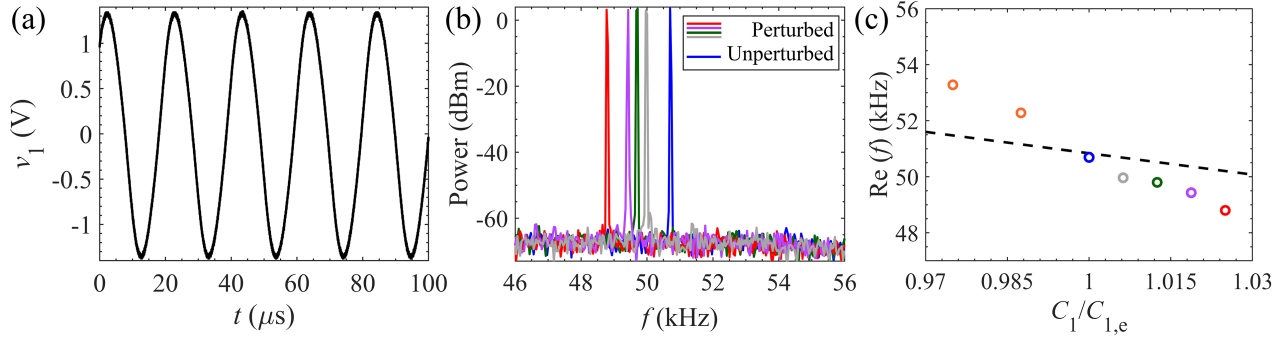


Fig. 8. (a) Measured time-domain voltage signal at the capacitor C_1 when the system is perturbed from the EPD by $C_1 - C_{1,0} = 2.5$ nF. (b) Measured capacitor voltage spectrum with the unperturbed frequency of oscillation of 50.7 kHz (blue); 49.96 kHz for perturbation $\Delta_C = 0.625$ % (gray); 49.8 kHz for $\Delta_C = 1.25$ % (green); 49.43 kHz for $\Delta_C = 1.875$ % (purple); and 48.9 kHz for $\Delta_C = 2.5$ % (red). (c) Comparison of the measured oscillation frequencies of the proposed nonlinear circuit (color dots) and those of the perturbed single LC linear circuit (dashed black line), when perturbing the positive capacitance.

a first perturbed frequency $|\Delta_f| = 1.46$ % for the smallest capacitance perturbation $\Delta_C = 0.625$ %. Hence, the gyrator-based EPD oscillator exhibits a sensitivity of $S = 2.34$, (for $\Delta_C = 0.625$ %.) which is comparable to or higher than the counterpart circuits as shown next. In the linear single LC resonator, the sensitivity shown in Fig. 8(c) is $S = 0.5$, hence it is lower than that of the proposed circuit oscillator.

In Ref. [10], they used a linear regime in a single time-varying resonator, and they measured a sensitivity of $|\Delta_f| = 0.66$ %, calculated based on the separation of the two perturbed resonance frequencies, for their smallest perturbation considered $\Delta_C = 0.3$ %, as shown in Fig. 6(a) of their paper. Thus, in [10], they achieved an approximate sensitivity of $S = 2.2$ for the first perturbation.

Sensitivity in the PT-symmetric two-coupled resonators in Ref. [13] was measured approximately as $S = 0.75$ in Fig. 2 of that paper with $|\Delta_f| = 5$ %, calculated based on the separation of the two resonance frequencies after perturbation, for their smallest applied perturbation of $\Delta_\gamma = 6.7$ % where in this case $X = \gamma = R^{-1}\sqrt{L/C}$. Therefore, the highest sensitivity measured in [13] was just slightly higher than that of a single linear LC resonator. Since experimental data at the EPD were not available, the sensitivity was calculated based on the frequency shift corresponding to perturbation of normalized γ approximately from 1.042 to 0.975. These two points correspond to the first perturbations occurring just before and after the EPD.

In Ref. [16], the authors used an oscillator scheme using a nonlinear saturated regime (analogous to what considered in this paper) in two-coupled resonators, and measured a frequency change of $|\Delta_f| = 1.29$ % for their smallest perturbation of $\Delta_C = 1.3$ %. Therefore, in [16], the sensitivity was measured to be $S = 0.99$.

In [15], the EPD concept using saturable nonlinear gain was exploited to design oscillators based on two coupled transmission lines as in [14]. They observe oscillation frequency changes in response to perturbations in the load resistance, so in this case we have $X = R$, and $\Delta_X = \Delta_R$. In their measurement (Fig. 16 in [15]), they observed a $|\Delta_f| = 20$ % for a resistance perturbation of $\Delta_R = 9.8$ %, resulting in a sensitivity of $S = 2.04$. Since experimental data at the EPD

were not available, the sensitivity was calculated based on the frequency shift obtained by perturbing the load resistance from 51 Ω to 56 Ω , relative to a fundamental frequency of 1 GHz.

Note that besides aiming at high sensitivity, another very important parameter is the *capability to detect small perturbations*. The measured capacitance variation $\Delta_C = 0.625$ % in the gyrator-based circuit in this paper is higher only than the case in Ref. [10] where $\Delta_C = 0.3$ %. Hence, the smallest perturbation in the gyrator-based oscillator is smaller than the one in [16] where $\Delta_C = 1.3$ %, and it is much smaller than the smallest variation in [13], $\Delta_\gamma = 6.7$ % (note that the low sensitivity measured in [13] probably depends on the large variation they considered, since the EPD-based sensitivity decreases when moving away from the EPD). Furthermore, the perturbation measured in [15] was $\Delta_R = 9.8$ %.

The capability to detect small variations Δ_X depends on both the *sensitivity* and the *linewidth* of the oscillator spectrum. The linewidth of the experimental oscillation frequency was measured to be only 10 Hz. However, such a linewidth could be even smaller than that measured value because we did not have the capability to use a narrower intermediate frequency bandwidth of the spectrum analyzer to test it.

Nonlinear effects such as gain saturation and Kerr nonlinearity in systems with EPD play an important role in sensitivity and stability [41]. The analysis of the nonlinear modes of the system can be carried over by resorting to nonlinear dynamics tools [42], where the modes of the system are identified as fixed points of the system equations. At the same time, the stability of such fixed points (ultimately determining whether the system will operate in those modes) is obtained from the Lyapunov exponents associated to the Jacobian matrix of the system equations linearized around the fixed point. Some dynamics related to EPDs in nonlinear systems are discussed in [43], [44], or more recently in the framework of electronic circuits, in [25] where a singularity is found in the nonlinear framework. In [25], they discussed the sensitivity of the system supporting the EPD and how nonlinearity helps the signal-noise ratio (how much noise contributes to the system). In this work, we do not focus on describing the system's nonlinearity but we observe the saturated regime using an implementation with electronic components. Based on the experimental results

shown in Fig. 8(b), which shows a clear and sharp spectrum, for each perturbed case, we conclude that our nonlinear system works effectively in the saturation regime, for each value of the perturbed capacitor.

IV. CONCLUSIONS

We have shown that two resonators connected via a gyrator support an EPD when one resonator is made of a negative inductance and a negative capacitance. We have provided the theoretical conditions for such EPD to exist at a purely real frequency and verified our theoretical calculations by using a time domain circuit simulator (Keysight ADS). We have demonstrated that the eigenfrequencies are exceptionally sensitive to a perturbation of the system and this may have significant implications for ultra-sensitive sensing technology and RF sensors. In addition, we show that the system has two complex eigenfrequencies, one of which is always associated to the circuit instability. We have fabricated the circuit and using the saturated regime, we have measured the sensitivity of the self-oscillation frequency to small capacitance perturbations. We have measured both the *sensitivity* and the *linewidth* of the oscillator's spectrum, because these two parameters are important for detecting small circuit perturbations. The spectrum exhibited a very narrow linewidth (i.e., 10 Hz), and the measured signal had a noise floor at -70 dB from the spectrum peak, and the circuit's sensitivity was measured to be comparable or better than cases previously published. We believe that the demonstrated concept of an oscillator in the saturated regime that is very sensitive to perturbations could pave the way for the development of new operation schemes to boost the performance of highly sensitive sensors.

V. APPENDIX

A. Circuits Duality

The concept of duality applies to many fundamental physics/engineering concepts. For instance, this concept has been utilized many times in electromagnetic and electric circuits. Two circuits are dual if the mesh equations that describe one of them have the same mathematical form as the nodal equations that characterize another circuit [45]. We consider the mesh equations in the parallel-parallel configuration using the Kirchhoff's voltage law. According to the duality theorem, if we substitute voltage by current, current by voltage, capacitance by inductance, and inductance by capacitance, we can obtain mesh equations for series-series configuration. Thus, we present a dual circuit of the parallel configuration, achieving an EPD by utilizing gyrator-based circuits with two series-series resonators.

1) *EPD in Lossy Series Circuit*: We analyze the EPD condition in the series-series configuration by accounting for series resistors R_1 and R_2 in both resonators. Using the Liouvillian formalism, the Kirchhoff voltage law equations for the two loops of the circuit in Fig. 9(a), and the state vector of $\Psi \equiv [Q_1, Q_2, \dot{Q}_1, \dot{Q}_2]^T$, we obtain

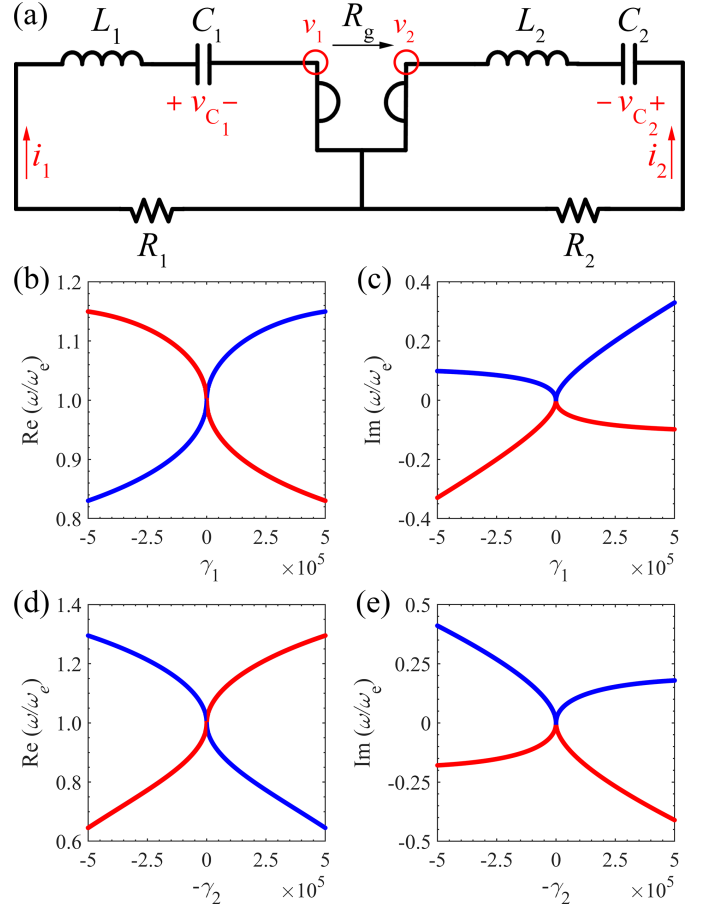


Fig. 9. (a) Schematic view of the lossy series-series configuration including a resistor in each resonator. The right resonator is made of negative inductance and capacitance. Variation of (b) real and (c) imaginary parts of the angular eigenfrequencies to a resistor perturbation in the left resonator. In these plots, γ_1 is varied whereas we assume $\gamma_2 = 0$. Variation of (d) real and (e) imaginary parts of the angular eigenfrequencies to a resistor perturbation on the right resonator. In these plots, $-\gamma_2$ is varied whereas we assume $\gamma_1 = 0$. In these plots, blue curves show stable branches with positive imaginary parts and red curves show unstable branches with negative imaginary parts. The right half of each plot demonstrates the variation in eigenfrequencies due to varying positive resistance, whereas the left half demonstrates the variation in eigenfrequencies due to varying negative resistance.

$$\frac{d\Psi}{dt} = \mathbf{M}\Psi, \quad \mathbf{M} = \begin{pmatrix} 0 & 0 & 1 & 0 \\ 0 & 0 & 0 & 1 \\ -\omega_{01}^2 & 0 & -\gamma_1 & \frac{R_g}{L_1} \\ 0 & -\omega_{02}^2 & -\frac{R_g}{L_2} & -\gamma_2 \end{pmatrix}, \quad (17)$$

where, $\gamma_1 = R_1/L_1$ and $\gamma_2 = R_2/L_2$ describe losses (losses on the right resonator are represented by a negative γ_2 since L_2 is negative). These eigenfrequencies are solutions to the following characteristic equation

$$\omega^4 - j\omega^3(\gamma_1 - \gamma_2) - \omega^2 \left(\omega_{01}^2 + \omega_{02}^2 + \gamma_1\gamma_2 + \frac{R_g}{L_1L_2} \right) + j\omega(\gamma_1\omega_{02}^2 + \gamma_2\omega_{01}^2) + \omega_{01}^2\omega_{02}^2 = 0. \quad (18)$$

An eigenfrequency with a negative imaginary part is associated with an exponentially growing signal. The coefficients of the odd-power terms of the angular eigenfrequency (ω and ω^3)

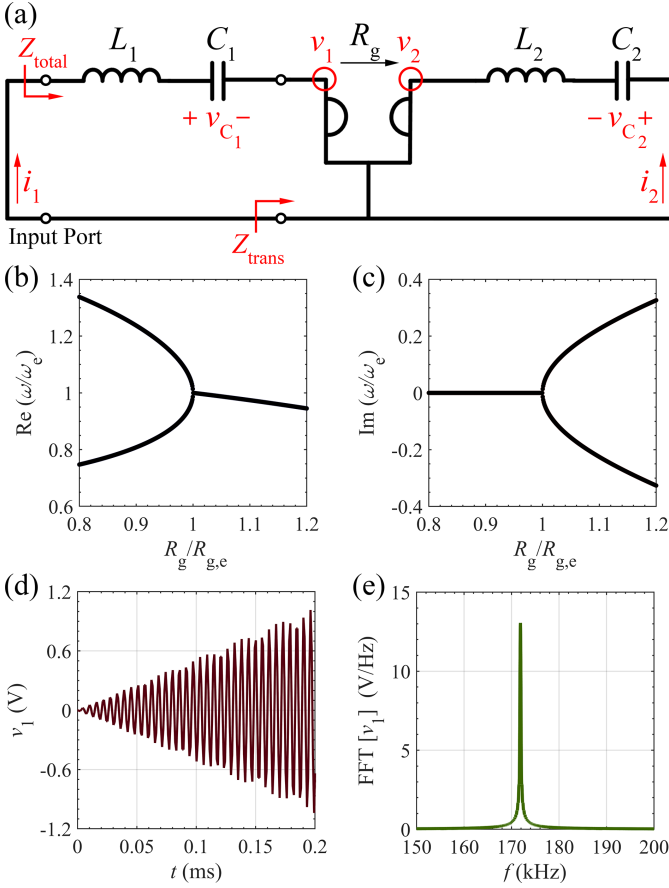


Fig. 10. (a) Series-series configuration: two different LC resonators in series configuration connected via an ideal gyrator. The right resonator is made of negative inductance and capacitance. Variation of the (b) real and (c) imaginary parts of the two eigenfrequencies to a gyration resistance perturbation. The bifurcation in the real part is observed for $R_g < R_{g,e}$. Voltage v_1 under the EPD condition in the (d) time domain, and (e) frequency domain. The frequency domain result is calculated from 150 kHz to 200 kHz with 10^6 samples in the time window between 0 ms to 0.2 ms.

in the characteristic equation of Eq. (18) are imaginary. In the characteristic equation, eigenfrequencies ω and $-\omega^*$ are both roots. In order to have a stable circuit with real-valued eigenfrequencies the odd-power terms of the angular eigenfrequency $-j\omega^3(\gamma_1 - \gamma_2)$ and $j\omega(\gamma_1\omega_{02}^2 + \gamma_2\omega_{01}^2)$ in the characteristic equation of Eq. (18) should be zero, otherwise a complex eigenfrequency needed to satisfy the characteristic equation of Eq. (18). The coefficient of the ω^3 term is zero when $\gamma_1 = \gamma_2$, and under this condition the coefficient of the ω term $\gamma_1(\omega_{02}^2 + \omega_{01}^2)$ is non-zero value because ω_{01}^2 and ω_{02}^2 are both positive. Moreover, the coefficient of the ω term vanishes when $\gamma_1/\gamma_2 = -\omega_{01}^2/\omega_{02}^2$, and under this condition, the coefficient of the ω^3 term $\gamma_1(1 + \omega_{02}^2/\omega_{01}^2)$ cannot vanish. Thus, it is not possible to have all real-valued coefficients in the characteristic polynomials, unless $\gamma_1 = \gamma_2 = 0$ which corresponds to a lossless circuit. In the following subsection, we examine the eigenfrequency in a lossless structure to understand its stability conditions.

2) *EPD in Lossless Series Circuit*: To have a real-valued EPD frequency and fulfill the EPD conditions, we suppose $\gamma_1 = \gamma_2 = 0$. In this configuration, two series LC resonators

are connected by a gyrator, as illustrated in Fig. 10(a). We assume that all components are ideal, and the circuit does not contain any resistance. By writing down the Kirchoff voltage law equations in two loops, we write the eigenvalue problem associated to the circuit equations, and the characteristic equation is obtained from $\det(\underline{\mathbf{M}} - j\omega\underline{\mathbf{I}}) = 0$, leading to

$$\omega^4 - \omega^2 \left(\omega_{01}^2 + \omega_{02}^2 + \frac{R_g}{L_1 L_2} \right) + \omega_{01}^2 \omega_{02}^2 = 0. \quad (19)$$

In this characteristic equation, ω is the angular eigenfrequency of the system. All the ω 's coefficients are real hence ω and ω^* are both roots of the characteristic equation, where $*$ represents the complex conjugate operation. Moreover, it is a quadratic equation in ω^2 ; therefore, ω and $-\omega$ are both solutions. For $R_g = 0$, the two resonators are uncoupled, and the two circuits have two angular eigenfrequency pairs of $\omega_{1,3} = \pm\omega_{01}$, and $\omega_{2,4} = \pm\omega_{02}$. We assume that the resonance frequency of each single LC resonator is real-valued; this happens when inductance and capacitance in the same resonator have both the same sign. In this case, the component values on the left side are positive, whereas they are negative on the right side. We explain the reason for this issue in Appendix V-B1. The angular eigenfrequencies (resonance frequencies) in the coupled circuit are calculated as

$$\omega_{1,3} = \pm\sqrt{a+b}, \quad \omega_{2,4} = \pm\sqrt{a-b}, \quad (20)$$

where

$$a = \frac{1}{2} \left(\omega_{01}^2 + \omega_{02}^2 + \frac{R_g}{L_1 L_2} \right), \quad (21)$$

$$b^2 = a^2 - \omega_{01}^2 \omega_{02}^2. \quad (22)$$

According to Eq. (20), the EPD condition requires

$$b = 0, \quad (23)$$

and the EPD angular frequency is $\omega_e = \pm\sqrt{a}$. Here, we assume positive values for a in order to have a real EPD angular frequency and we will only refer to positive values of ω_e in the following. From Eq. (22), the EPD condition is rewritten as $a^2 = \omega_{01}^2 \omega_{02}^2$. Since we look for real-valued EPD frequencies, $a > 0$, and from Eq. (21) one has

$$\omega_{01}^2 + \omega_{02}^2 - \omega_{gs}^2 > 0, \quad (24)$$

where it has been convenient to define the equivalent gyrator frequency $\omega_{gs}^2 = -R_g/(L_1 L_2)$ for the series-series configuration (note that $\omega_{gs}^2 > 0$ because one inductor is negative). The EPD frequency is calculated by using Eqs. (21), (22), and (23) as

$$\omega_e = \sqrt{\frac{1}{2} (\omega_{01}^2 + \omega_{02}^2 - \omega_{gs}^2)} = \sqrt{\omega_{01} \omega_{02}}. \quad (25)$$

3) *Dispersion Relation of Lossless and Lossy Series-Series Configurations*: As an example, we explain the required procedure to obtain an EPD in this configuration by presenting a specific example. Many different combinations of values for the circuit's components will satisfy the EPD condition, and here as an example, we assume this set of values for components: $L_1 = 47 \mu\text{H}$, $L_2 = -47 \mu\text{H}$, $C_2 = -47 \text{nF}$, and $R_g = 50 \Omega$. As mentioned before, the desired value for the gyration resistance is achieved by determining the appropriate values for the resistors in the circuit for the gyration illustrated in Fig. 6(b). Also, the capacitance C_1 is determined by solving the quadratic equation from the EPD condition in Eq. (23). There are two different values of the capacitance C_1 in the first resonator that satisfy Eq. (23), namely $C_{1,e} = 7.05 \text{nF}$ and $C_{1,e} = 139.16 \text{nF}$. For the smaller value ($C_{1,e} = 7.05 \text{nF}$), we obtain a positive value for a in Eq. (24), so the EPD frequency is real. On the contrary, the second value ($C_{1,e} = 139.16 \text{nF}$) gives us a negative value for a , so the EPD frequency would be imaginary and we discard it since we investigate a gyration-based circuit with real-valued EPD frequency in this paper. In the following, we select the smaller value for the left resonator capacitance, $C_1 = 7.05 \text{nF}$. The results in Figs. 10(b) and (c) exhibit the two branches of the real and imaginary parts of perturbed eigenfrequencies obtained from the eigenvalue problem, varying the gyration resistance R_g in the neighborhood of $R_{g,e} = 50 \Omega$. Here, only the two solutions with $\text{Re}(\omega) > 0$ are shown in Figs. 10(b) and (c). In this example, we obtain $\omega_e = 1.08 \times 10^6 \text{ rad/s}$ and the coalesced eigenvalues at EPD are exceedingly sensitive to perturbations in system parameters.

The time domain simulation results obtained using the Keysight ADS circuit simulator are illustrated in Figs. 10(d) and (e). These two plots show the voltage $v_1(t)$ in the left resonator, and its spectrum, where we put 1 mV as an initial voltage on C_1 . In the circuit simulator, an ideal gyration has been utilized. According to Fig. 10(d), the voltage grows linearly with increasing time. This important aspect is peculiar of an EPD, and it is the result of coalescing system eigenvalues and eigenvectors that also corresponds to a double pole in the system. A linear growth indicates a second-order EPD in the system. We take a fast Fourier transform (FFT) of the voltage $v_1(t)$ to show the frequency spectrum, and the calculated result is illustrated in Fig. 10(e). The observed oscillation frequency is $f_o = 172.05 \text{ kHz}$, which is in good agreement with the theoretical value $\omega_e/(2\pi)$ calculated above.

By perturbing the gyration resistance, the operation point moves away from the EPD. By selecting a lower value for the gyration resistance, the system has two different real-valued eigenfrequencies. For instance, we reduce the amount of perturbed parameter by 5% equal to $R_g = 47.5 \Omega < R_{g,e} = 50 \Omega$. In the perturbed condition, we do not observe any signal growth in the system with increasing time. If we consider an additive 5% of perturbation in the gyration resistance, i.e., $R_g = 52.5 \Omega > R_{g,e} = 50 \Omega$, the imaginary part of the angular eigenfrequencies is non-zero, and it causes eigensolutions with damping and growing signals in the system. Since the signal is in the form of $Q_n \propto e^{j\omega t}$, the eigenfrequency with negative imaginary part is associated to an exponentially

growing signal.

In lossy circuit, we use the same values as lossless series-series configuration for the resonators and gyration resistance. In Figs. 9(b) and (c), γ_1 is varied while we assume $\gamma_2 = 0$. In Figs. 9(d) and (e), $-\gamma_2$ is perturbed while $\gamma_1 = 0$. These two figures show the real and imaginary parts of eigenfrequencies when perturbing each resistor individually. The EPD angular frequency is obtained when $\gamma_1 = \gamma_2 = 0$, which is the same EPD frequency as the lossless configuration shown in Section V-A2. In Figs. 9(b)-(e), we observe the bifurcations of the real and imaginary parts of the eigenfrequencies, so the circuit is very sensitive to variations in both resistance values. Angular eigenfrequencies here are complex-valued; it means that by perturbing γ_1 or γ_2 away from $\gamma_1 = \gamma_2 = 0$, the circuit gets unstable; hence it starts to oscillate with the fundamental frequency associated with the real part of the unstable angular eigenfrequency. When γ_1 or γ_2 is perturbed from the EPD value, the oscillation frequency is shifted from the EPD frequency, and it could be measured for sensing applications. In Figs. 9(b)-(e), both conditions $\gamma_1 > 0$ and $-\gamma_2 > 0$ represent losses, whereas the conditions $\gamma_1 < 0$ and $-\gamma_2 < 0$ represent gains in the circuit through a negative resistance. In both cases, by adding either losses or gains, the system is unstable. We observe more sensitivity when perturbing R_2 , because a small perturbation in R_2 results in a larger variation of the eigenfrequencies than when varying R_1 . Indeed, a wider bifurcation indicates higher sensitivity.

4) *Frequency Domain Analysis of The Degenerate Resonance*: We calculate the total input impedance, $Z_{\text{total}}(\omega)$ (see Fig. 10), for the series-series circuit with the same approach discussed in the Section II-E. We calculate the transferred impedance on the left side of the circuit in Fig. 10, that is

$$Z_{\text{trans}}(\omega) = \frac{R_g^2}{Z_2}. \quad (26)$$

where $Z_2(\omega) = j\omega L_2 + 1/(j\omega C_2)$ is the series impedance on the right side of the circuit. Thus, the total impedance observed from the input port in this circuit is calculated by

$$Z_{\text{total}}(\omega) \triangleq Z_1(\omega) + Z_{\text{trans}}(\omega) = Z_1 + \frac{R_g^2}{Z_2}, \quad (27)$$

as shown in Fig. 10, where $Z_1(\omega) = j\omega L_1 + 1/(j\omega C_1)$. The complex-valued resonant frequencies are obtained by imposing $Z_{\text{total}}(\omega) = 0$. A few steps lead to the ω -zeros given by Eq. (20). Figure 11 shows the zeros of such total impedance $Z_{\text{total}}(\omega)$ for various gyration resistance values. When considering the EPD gyration resistance $R_g = R_{g,e} = 50 \Omega$, one has $Z_{\text{total}}(\omega) \propto (\omega - \omega_e)^2$, i.e., the two zeros coincide with the EPD angular frequency ω_e , that is also the point where the two curves in Fig. 11 meet. For gyration resistances such that $R_g < R_{g,e}$, the two resonance angular frequencies are purely real. Instead, for $R_g > R_{g,e}$, the two resonance angular frequencies are complex conjugate, consistent with the result in Fig. 11. In other words, the EPD frequency coincides with double zeros or double poles of the frequency spectrum, depending on the way the circuit is described.

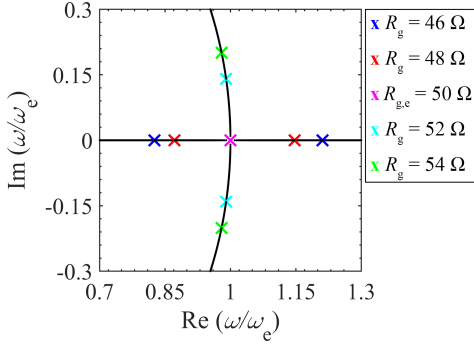


Fig. 11. Root locus of zeros of $Z_{\text{total}}(\omega)$ of the series-series configuration when varying the gyration resistance. The EPD frequency corresponds to a double zero of the impedance $Z_{\text{total}}(\omega)$.

B. Components Sign and Simplification of EPD Condition

1) *Series-Series Configuration*: In order to obtain an EPD in the series-series configuration using Eqs. (21), (22) and (23) the following equation must be satisfied:

$$(\omega_{01} - \omega_{02})^2 = \omega_{\text{gs}}^2. \quad (28)$$

We investigate three possible scenarios to satisfy Eq. (28). First, if ω_{01} and ω_{02} are pure real, the values of L_1 or L_2 should be negative to have the same sign on both sides of Eq. (28). Thus, one of the resonators should have a negative inductance to have a pure real ω_{01} or ω_{02} . Second, if both ω_{01} and ω_{02} have imaginary values, the considered values for L_1 and L_2 should have the same sign, either positive or negative. When L_1 and L_2 are positive, C_1 and C_2 should be negative or vice versa. Finally, if just one of the ω_{01} or ω_{02} is imaginary and the other one has a real value, there are no conditions to obtain an EPD.

To have a real EPD frequency $\omega_e = \pm\sqrt{a}$, a should be positive and this happens when Eq. (24) is satisfied. The region leading to $a > 0$ is represented by the white area in Fig. 12(a), whereas the gray area represents the region with $a < 0$. The red curves show different combinations of ω_{01} and ω_{02} which satisfy the EPD condition of Eq. (28), assuming ω_{gs} constant. In this figure, $C_1 = 1/(\omega_{01}^2 L_1)$ and $C_2 = 1/(\omega_{02}^2 L_2)$ are varied, while R_g , L_1 and L_2 are constant. We have shown only results for positive real values of ω_{01} and ω_{02} . The green cross marks the values used for the example provided in Section V-A2.

2) *Parallel-Parallel Configuration*: In order to get an EPD in the parallel-parallel configuration by using Eqs. (6), (7) and (8) the following condition must be satisfied:

$$(\omega_{01} - \omega_{02})^2 = \omega_{\text{gp}}^2. \quad (29)$$

We consider three different cases for the parallel-parallel configuration to choose the components' values. First, if ω_{01} and ω_{02} are pure real, the values of C_1 or C_2 should be negative to have the same sign on both sides of Eq. (29). Hence, to have a real ω_{01} and ω_{02} one resonator should be made of both negative C and L . Second, if both ω_{01} and ω_{02} have imaginary values, then C_1 and C_2 should have the same sign. Finally, if just one of the ω_{01} or ω_{02} is imaginary and

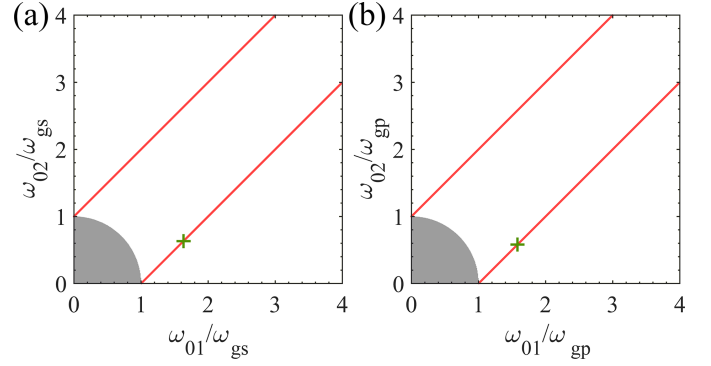


Fig. 12. Possible combinations of ω_{01} and ω_{02} to have a real eigenfrequency in the (a) series-series and (b) parallel-parallel configurations are shown by the white area, and the gray area represents complex eigenfrequencies based on (a) Eq. (24) for series-series configuration and (b) Eq. (9) for parallel-parallel configuration. Red curves satisfy (a) Eq. (28) for series-series configuration and (b) Eq. (29) for parallel-parallel configuration and show possible combinations of ω_{01} and ω_{02} that lead to a real EPD frequency. In the results presented in plot (a), we keep R_g , L_1 and L_2 fixed as in Section V-A2, and C_1 and C_2 are varied. In the results presented in plot (b), we keep R_g , C_1 and C_2 fixed as in Section II-B, and L_1 and L_2 are varied.

the other is real, there is no condition that leads to an EPD. In this paper, we consider the first scenario, where both ω_{01} and ω_{02} are real.

To have a real EPD frequency $\omega_e = \pm\sqrt{a}$, a should be positive and this occurs when Eq. (9) is satisfied. The region leading to $a > 0$ is represented by the white area in Fig. 12(b), whereas the gray area represents the region with $a < 0$. The red curves show different combinations of ω_{01} and ω_{02} which satisfy the EPD condition of Eq. (29), assuming ω_{gp} constant. In this figure, $L_1 = 1/(\omega_{01}^2 C_1)$ and $L_2 = 1/(\omega_{02}^2 C_2)$ are varied, while R_g , C_1 and C_2 are constants. We show only results for the positive and real values of ω_{01} and ω_{02} . The points on the red curves, which are located in the white area, can be selected to have an EPD with real and positive EPD frequency. The location marked by the green cross shows the values used for the example in Subsection II-B.

C. The Coefficient of The Leading Term of The Puiseux Series

Using Eq. (13), we obtain the following expression for the coefficient of the leading term of the Puiseux series,

$$\alpha_1 = \sqrt{\frac{\omega_{01}^2 R_g (\omega_e - \omega_{02}^2) + \frac{\omega_e}{C_1 C_2}}{\frac{1}{C_1 C_2} + R_g (\omega_{01}^2 + \omega_{02}^2 - 6\omega_e)}}, \quad (30)$$

when we perturb the capacitance. Instead, when we perturb the inductance, the coefficient is

$$\alpha_1 = \sqrt{\frac{\omega_{01}^2 R_g (\omega_e - \omega_{02}^2)}{\frac{1}{C_1 C_2} + R_g (\omega_{01}^2 + \omega_{02}^2 - 6\omega_e)}}. \quad (31)$$

D. The Impedance Inverter

There are several circuits that can provide for negative capacitances and inductances needed for the gyration-based EPD circuits. Two circuits to obtain negative impedances by using op amps are shown in Fig. 13. The circuit in Fig. 13(a) converts the impedance $Z_{\text{Load}}(\omega)$ to $Z_{\text{in}}(\omega) = -Z_{\text{Load}}(\omega)$.

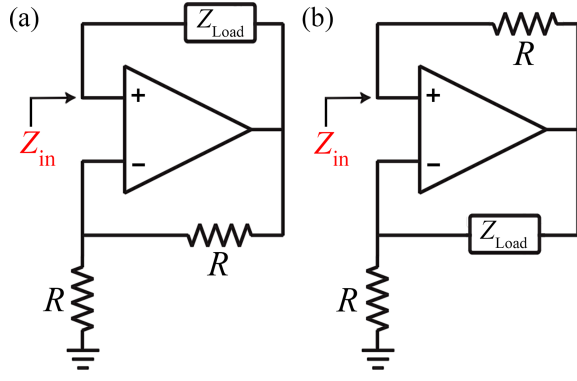


Fig. 13. Negative impedance converter circuit implementations by using an op amp. (a) Circuit used in the experimental setup where the load is the parallel between a positive capacitor and a positive inductor. (b) A negative inductance can be generated using a positive capacitor (not used in the experimental setup).

Therefore, when $Z_{\text{Load}}(\omega)$ in the circuit in Fig. 13(a) is a capacitor in parallel to an inductor, i.e., $Z_{\text{Load}}(\omega) = 1/(j\omega C) \parallel (j\omega L)$, we obtain $Z_{\text{in}}(\omega) = -(1/(j\omega C) \parallel (j\omega L))$ at the input port, that corresponds to a negative capacitor in parallel to a negative inductor. In Sec. III, we used this method to realize negative capacitance and inductance in the measurement. Figure 13(b) shows an alternative way to achieve negative inductance without an inductor. By using a single capacitor in the mentioned inverter $Z_{\text{Load}}(\omega) = 1/(j\omega C)$ resulting in $Z_{\text{in}}(\omega) = -j\omega R^2 C$, hence, desired negative inductance values are achieved with proper sets of values for R and C . Therefore, it is possible to generate a negative capacitance and a negative inductance by only using capacitive loads.

E. Implementation of The Gyration-based Circuit

Assembled gyration-based circuit with different blocks highlighted is shown in Fig. 14. The green dashed square shows the designed gyration using two op amps, and the red dashed square shows the inverter circuit to provide a negative inductor in parallel to a negative capacitor. The circuit also consists of a sensing capacitor C_1 , where a variable capacitor (FTVOGUE, model Variable Capacitance Kit) and a series of extra capacitors could be connected in parallel, as shown in the blue box. To demonstrate the sensitivity of the oscillator's frequency to perturbations, we perturb the capacitor C_1 by connecting pairs of extra 2.5 nF capacitors in parallel to C_1 . After each perturbation, the oscillation frequency is measured using an oscilloscope and a spectrum analyzer for comparison and verification purposes. Note that on the board, all elements and the DC supply share a common ground and the VSS (-5 V) and VCC ($+5$ V) are connected to op amps as shown in Fig. 14.

ACKNOWLEDGMENT

This material is based upon work supported by the National Science Foundation (NSF) under Grant No. ECCS-1711975 and by Air Force Office of Scientific Research (AFOSR) under Grant No. FA9550-19-1-0103.

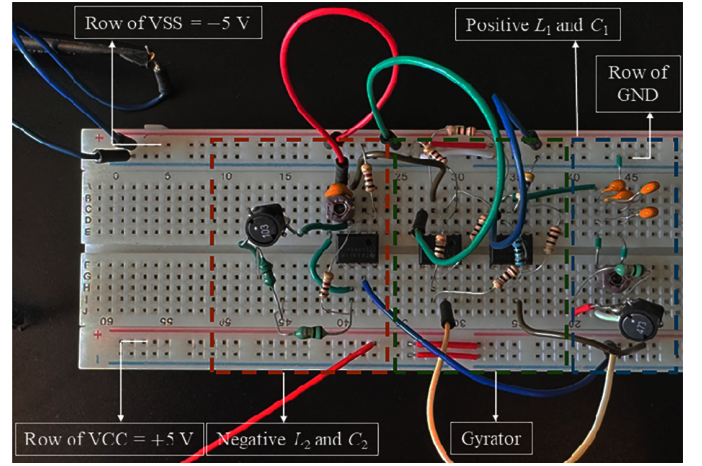


Fig. 14. Assembled gyration-based oscillator circuit prototype with different blocks highlighted.

REFERENCES

- [1] M. I. Vishik and L. A. Lyusternik, "The solution of some perturbation equations for matrices and selfadjoint or non-selfadjoint differential equations I," *Russian Mathematical Surveys*, vol. 15, no. 3, p. 1, 1960.
- [2] P. Lancaster, "On eigenvalues of matrices dependent on a parameter," *Numerische Mathematik*, vol. 6, no. 1, pp. 377–387, 1964.
- [3] T. Kato, *Perturbation Theory for Linear Operators*. Springer-Verlag New York Inc., New York, 1966.
- [4] W. Heiss and A. Sannino, "Avoided level crossing and exceptional points," *Journal of Physics A: Mathematical and General*, vol. 23, no. 7, p. 1167, 1990.
- [5] A. P. Seyranian, "Sensitivity analysis of multiple eigenvalues," *Mechanics of Structures and Machines*, vol. 21, no. 2, pp. 261–284, 1993.
- [6] C. M. Bender, M. Berry, and A. Mandilara, "Generalized PT symmetry and real spectra," *Journal of Physics A: Mathematical and General*, vol. 35, no. 31, p. L467, 2002.
- [7] W. Heiss, "Exceptional points of non-Hermitian operators," *Journal of Physics A: Mathematical and General*, vol. 37, no. 6, p. 2455, 2004.
- [8] A. Seyranian, O. Kirillov, and A. Mailybaev, "Coupling of eigenvalues of complex matrices at diabolic and exceptional points," *Journal of Physics A: Mathematical and General*, vol. 38, no. 8, p. 1723, 2005.
- [9] W. D. Heiss, "The physics of exceptional points," *Journal of Physics A: Mathematical and Theoretical*, vol. 45, no. 44, p. 444016, oct 2012.
- [10] H. Kazemi, M. Y. Nada, A. Nikzamid, F. Maddaleno, and F. Capolino, "Experimental demonstration of exceptional points of degeneracy in linear time periodic systems and exceptional sensitivity," *Journal of Applied Physics*, vol. 131, no. 14, 2022.
- [11] A. Nikzamid, K. Rouhi, A. Figotin, and F. Capolino, "Time modulation to manage and increase the power harvested from external vibrations," *Applied Physics Letters*, vol. 123, no. 21, 2023.
- [12] C. M. Bender and S. Boettcher, "Real spectra in non-hermitian hamiltonians having PT symmetry," *Physical review letters*, vol. 80, no. 24, p. 5243, 1998.
- [13] J. Schindler, A. Li, M. C. Zheng, F. M. Ellis, and T. Kottos, "Experimental study of active LRC circuits with PT symmetries," *Physical Review A*, vol. 84, no. 4, p. 040101, 2011.
- [14] H. Kazemi, A. Nikzamid, T. Mealy, A. Abdelshafy, and F. Capolino, "High-sensitive parity-time symmetric oscillator in coupled transmission lines with nonlinear gain," *IEEE Journal of Microwaves*, vol. 2, no. 3, pp. 389–400, 2022.
- [15] C. Moncada, F. Ramirez, and A. Suárez, "Frequency-domain analysis of an oscillator with an exceptional point of degeneracy," *IEEE Transactions on Microwave Theory and Techniques*, 2024.
- [16] A. Nikzamid and F. Capolino, "Highly sensitive coupled oscillator based on an exceptional point of degeneracy and nonlinearity," *Physical Review Applied*, vol. 18, no. 5, p. 054059, 2022.
- [17] M. V. Berry, "Physics of nonhermitian degeneracies," *Czechoslovak journal of physics*, vol. 54, no. 10, pp. 1039–1047, 2004.
- [18] J. Wiersig, "Enhancing the sensitivity of frequency and energy splitting detection by using exceptional points: application to microcavity sensors

- for single-particle detection,” *Physical review letters*, vol. 112, no. 20, p. 203901, 2014.
- [19] K. Rouhi, R. Marosi, T. Mealy, A. F. Abdelshafy, A. Figotin, and F. Capolino, “Exceptional degeneracies in traveling wave tubes with dispersive slow-wave structure including space-charge effect,” *Applied physics letters*, vol. 118, no. 26, 2021.
- [20] K. Rouhi, F. Capolino, and A. Figotin, “Simple reciprocal electric circuit exhibiting exceptional point of degeneracy,” *Journal of Physics A: Mathematical and Theoretical*, 2024.
- [21] W. Chen, Ş. Kaya Özdemir, G. Zhao, J. Wiersig, and L. Yang, “Exceptional points enhance sensing in an optical microcavity,” *Nature*, vol. 548, no. 7666, pp. 192–196, 2017.
- [22] W. Chow, J. Gea-Banacloche, L. Pedrotti, V. Sanders, W. Schleich, and M. Scully, “The ring laser gyro,” *Reviews of Modern Physics*, vol. 57, no. 1, p. 61, 1985.
- [23] S. Sunada and T. Harayama, “Design of resonant microcavities: application to optical gyroscopes,” *Optics express*, vol. 15, no. 24, pp. 16 245–16 254, 2007.
- [24] P. Djorwe, Y. Pennec, and B. Djafari-Rouhani, “Exceptional point enhances sensitivity of optomechanical mass sensors,” *Physical Review Applied*, vol. 12, no. 2, p. 024002, 2019.
- [25] A. Suntharalingam, L. Fernández-Alcázar, R. Kononchuk, and T. Kottos, “Noise resilient exceptional-point voltmeters enabled by oscillation quenching phenomena,” *Nature Communications*, vol. 14, no. 1, p. 5515, 2023.
- [26] K. Bai, T.-R. Liu, L. Fang, J.-Z. Li, C. Lin, D. Wan, and M. Xiao, “Observation of nonlinear exceptional points with a complete basis in dynamics,” *Physical Review Letters*, vol. 132, no. 7, p. 073802, 2024.
- [27] A. Figotin, “Synthesis of lossless electric circuits based on prescribed Jordan forms,” *Journal of Mathematical Physics*, vol. 61, no. 12, 2020.
- [28] A. Figotin, “Perturbations of circuit evolution matrices with Jordan blocks,” *Journal of Mathematical Physics*, vol. 62, no. 4, 2021.
- [29] K. Rouhi, A. Nikzamir, A. Figotin, and F. Capolino, “Exceptional point in a degenerate system made of a gyration and two unstable resonators,” *Physical Review A*, vol. 105, no. 3, p. 032214, 2022.
- [30] K. Rouhi, A. Nikzamir, A. Figotin, and F. Capolino, “High-sensitivity in various gyration-based circuits with exceptional points of degeneracy,” *EPJ Applied Metamaterials*, vol. 9, 2022.
- [31] C. R. White, J. W. May, and J. S. Colburn, “A variable negative-inductance integrated circuit at uhf frequencies,” *IEEE Microwave and Wireless Components Letters*, vol. 22, no. 1, pp. 35–37, 2011.
- [32] A. Larky, “Negative-impedance converters,” *IRE Transactions on Circuit Theory*, vol. 4, no. 3, pp. 124–131, 1957.
- [33] P. Horowitz, W. Hill, and I. Robinson, *The art of electronics*. Cambridge university press Cambridge, 1989, vol. 2.
- [34] M. Ershov, H. Liu, L. Li, M. Buchanan, Z. Wasilewski, and A. K. Jonscher, “Negative capacitance effect in semiconductor devices,” *IEEE Transactions on Electron devices*, vol. 45, no. 10, pp. 2196–2206, 1998.
- [35] B. D. Tellegen, “The gyration, a new electric network element,” *Philips Res. Rep.*, vol. 3, no. 2, pp. 81–101, 1948.
- [36] R. M. Inigo, “Gyration realization using two operational amplifiers,” *IEEE Journal of Solid-State Circuits*, vol. 6, no. 2, pp. 88–89, 1971.
- [37] C. L. Hogan, “The ferromagnetic Faraday effect at microwave frequencies and its applications,” *Reviews of Modern Physics*, vol. 25, no. 1, p. 253, 1953.
- [38] B. Shenoï, “Practical realization of a gyration circuit and RC-gyration filters,” *IEEE Transactions on Circuit Theory*, vol. 12, no. 3, pp. 374–380, 1965.
- [39] A. Welters, “On explicit recursive formulas in the spectral perturbation analysis of a Jordan block,” *SIAM journal on matrix analysis and applications*, vol. 32, no. 1, pp. 1–22, 2011.
- [40] H. Hodaï, A. U. Hassan, S. Wittek, H. Garcia-Gracia, R. El-Ganainy, D. N. Christodoulides, and M. Khajavikhan, “Enhanced sensitivity at higher-order exceptional points,” *Nature*, vol. 548, no. 7666, pp. 187–191, 2017.
- [41] V. V. Konotop, J. Yang, and D. A. Zezyulin, “Nonlinear waves in PT-symmetric systems,” *Reviews of Modern Physics*, vol. 88, no. 3, p. 035002, 2016.
- [42] Y. A. Kuznetsov, I. A. Kuznetsov, and Y. Kuznetsov, *Elements of applied bifurcation theory*. Springer, 1998, vol. 112.
- [43] Y. Zhiyenbayev, Y. Kominis, C. Valagiannopoulos, V. Kovanis, and A. Bountis, “Enhanced stability, bistability, and exceptional points in saturable active photonic couplers,” *Physical Review A*, vol. 100, no. 4, p. 043834, 2019.
- [44] S. Yu, X. Piao, and N. Park, “Neuromorphic functions of light in parity-time-symmetric systems,” *Advanced Science*, vol. 6, no. 15, p. 1900771, 2019.
- [45] N. Balabanian, S. Seshu, and T. A. Bickart, *Electrical network theory*. Wiley, 1969.